Visual Neuroscience (1997), **14**, 507–522. Printed in the USA.
Copyright © 1997 Cambridge University Press 0952-5238/97 $11.00 + .10

Physiology of the A1 amacrine: A spiking, axon-bearing interneuron of the macaque monkey retina

DONNA K. STAFFORD AND DENNIS M. DACEY
Department of Biological Structure, University of Washington, Seattle

(RECEIVED April 15, 1996; ACCEPTED September 13, 1996)

Abstract

We characterized the light response, morphology, and receptive-field structure of a distinctive amacrine cell type (Dacey, 1989), termed here the A1 amacrine, by applying intracellular recording and staining methods to the macaque monkey retina *in vitro*. A1 cells show two morphologically distinct components: a highly branched and spiny dendritic tree, and a more sparsely branched axon-like tree that arises from one or more hillock-like structures near the soma and extends for several millimeters beyond the dendritic tree. Intracellular injection of Neurobiotin reveals an extensive and complex pattern of tracer coupling to neighboring A1 amacrine cells, to two other amacrine cell types, and to a single ganglion cell type. The A1 amacrine is an ON–OFF cell, showing a large (10–20 mV) transient depolarization at both onset and offset of a photopic, luminance modulated stimulus. A burst of fast, large-amplitude (~60 mV) action potentials is associated with the depolarizations at both the ON and OFF phase of the response. No evidence was found for an inhibitory receptive-field surround. The spatial extent of the ON–OFF response was mapped by measuring the strength of the spike discharge and/or the amplitude of the depolarizing slow potential as a function of the position of a bar or spot of light within the receptive field. Receptive fields derived from the slow potential and associated spike discharge corresponded in size and shape. Thus, the amplitude of the slow potential above spike threshold was well encoded as spike frequency. The diameter of the receptive field determined from the spike discharge was ~10% larger than the spiny dendritic field. The correspondence in size between the spiking receptive field and the spiny dendritic tree suggests that light driven signals are conducted to the soma from the dendritic tree but not from the axon-like arbor. The function of the axon-like component is unknown but we speculate that it serves a classical output function, transmitting spikes distally from initiation sites near the soma.

Keywords: Macaque monkey retina, Amacrine cells, Spikes, Tracer coupling

Introduction

Retinal amacrine cells are traditionally considered to be axonless interneurons, yet the morphology of a number of amacrine cell types challenges this view. Distinctive dendritic and axon-like components have been described on multiple amacrine cell types in different species (Catsicas et al., 1987; Sagar, 1987; Teranishi et al., 1987; Djamgoz et al. 1988; Dacey, 1988; Vaney et al., 1988; Ammermüller & Weiler, 1989; Dacey, 1989; Djamgoz et al., 1989; Djamgoz & Vallerga, 1989; Dacey, 1990*a,b,c*; White et al., 1990; Famiglietti, 1990, 1992*a,b*). These cell types all have a smaller dendritic tree that gives rise to a second, larger arbor that projects for long distances in the inner retina. For a given cell type, the axon-like processes arise from either the distal or proximal dendrites, or directly from the cell body; there may be a single axon-like process or several of them. The degree to which this anatomical interpretation reflects the functional polarization into a receptive dendritic tree and a transmitting axonal output remains speculative.

The physiology of amacrine cells is not well understood, but the earliest intracellular recordings revealed transient, spike-like depolarizations in the light responses of at least some amacrine cells (Werblin & Dowling, 1969; Kaneko, 1970; Matsumoto & Naka, 1972; Werblin, 1972). The amacrine cell spikes are generated by a tetrodotoxin (TTX) sensitive sodium current (Miller & Dacheux, 1976; Bloomfield, 1996). One line of evidence suggests that some amacrine cell spikes are regenerative potentials that can serve as an electrical boost, transmitting signals from remote distal dendrites towards the soma (Bloomfield, 1996; Freed et al., 1996). Amacrine cell spikes may also originate near the soma and propagate away from the cell body *via* long processes (Cook & Werblin, 1994), and thereby play a role in long-range, lateral inhibition (Werblin, 1972; Werblin & Copenhagen, 1974; Maguire et al., 1989).

Are spikes found in amacrine cells with axon-like processes? Several morphologically distinct types of spiking amacrine cells have been identified in rabbit retina (Bloomfield, 1991, 1992) but

Reprint requests to: Dennis Dacey, University of Washington, Department of Biological Structure, Box 357420, Seattle, WA 98195-7420, USA.

distinctive axon-like morphology was not observed. More recently, evidence for a link between axon-like processes and spiking in two rabbit amacrine cells has been given (Taylor, 1996). A problem is that it has been technically difficult to characterize clearly both the physiological response and the detailed morphology of any amacrine type. For example, the cholinergic, starburst amacrine is well characterized morphologically; it clearly does not bear both dendritic and long-range axon-like components (Famiglietti, 1983; Tauchi & Masland, 1984), but there is disagreement as to whether or not this cell generates dendritic spikes (Miller & Bloomfield, 1983; Jensen, 1995; Taylor & Wässle, 1995; Peters & Masland, 1996). In the present study, we characterize the light response and receptive-field structure of a distinctive "axon-bearing" amacrine cell type, termed here the A1 cell, recently identified in the retina of the macaque monkey (Dacey, 1989) (see Fig. 1). The A1 amacrine has a conventional, easily demarcated dendritic tree: the dendrites are spiny and form a highly branched, radially symmetrical field that is ~400 μm in diameter in the retinal periphery. In addition, one to three axon-like processes arise near the soma from distinct hillock-like thickenings and project beyond the dendritic tree to form a second, more sparsely branching and wide ranging arbor that surrounds the dendritic field to a diameter of over 4 mm. The axon-like processes are thin and smooth and bear distinct varicosities along their lengths.

We show here that the A1 cell is a clear example of a spiking amacrine: a burst of fast, large-amplitude spikes is elicited at both light onset and offset. We found the strength of synaptic input, as measured by the amplitude of the slow potential, was reliably encoded as spike discharge frequency; the spiking output could therefore be used to map the spatial extent of both the ON and OFF responses. Receptive-field diameter approximates the diameter of the spiny dendritic tree. The widespreading axon-like field does not contribute a detectable excitatory input to the receptive field. We hypothesize that the receptive field of the A1 cell is determined primarily by spatial summation of synaptic input to the spiny dendritic tree and that the spikes do not transmit signals from the widespreading axon-like tree to the soma. The function of the axon-like arbor and the origin and direction of propagation of the large-amplitude spikes is not known, but we speculate that axon-like arbor serves an output function and that the spikes originate at the origins of the axons, near the soma and propagate distally along the axon-like processes.

Materials and methods

This study is based on results from eyes of *Macaca nemestrina* (n = 78), *Macaca fascicularis* (n = 8), and *Macaca mulatta* (n = 1) obtained through the Tissue Program of the Regional Primate Center at the University of Washington. No obvious differences were found in the data taken from the three species so these data were combined in the present Results.

In vitro preparations

Two different *in vitro* preparations of the macaque retina were used to study the morphology and physiology of primate retinal neurons. The first preparation was designed for anatomical characterization using intracellular staining techniques, and has been described previously (Dacey & Brace, 1992; Dacey, 1993). In brief, whole eyes were removed immediately after euthanasia and retinas were dissected free of the vitreous and the eyecup in oxygenated culture medium (Ames; Sigma, Buchs, Switzerland). The retinas were then placed flat, vitreal side up, in a superfusion chamber that was mounted on the stage of a light microscope. The isolated retina was maintained *in vitro* at room temperature. For intracellular filling, fine-tipped, low-resistance intracellular microelectrodes were formed from thin-walled microcapillary glass (Sutter Instruments, Novato, CA) and filled with a solution of 4% Neurobiotin (Vector Labs., Burlingame, CA) and 1–2% Lucifer Yellow (Aldrich Chemical, Milwaukee, WI) in MOPS buffer (Sigma, Buchs, Switzerland; 20 mM, pH 7.6) to give an initial resistance of ~100 MΩ. The electrodes were beveled to a final resistance of ~50 MΩ.

A second, modified *in vitro* preparation permitted analysis of both anatomical and physiological properties (Dacey & Lee, 1994; Dacey et al., 1996). In this preparation the retina, choroid, and retinal pigment epithelial (RPE) layers were dissected from the eyecup as an intact unit. The retina-choroid-rpe was placed in a chamber equipped with a temperature controller (ATR4; Quest Scientific, La Jolla, CA). Temperature of the superfusate was maintained at 36 ± 0.1°C. For combined intracellular recording and staining, microelectrodes were filled with a solution of 2–3% Neurobiotin and 1–2% Pyranine (Molecular Probes, Eugene, OR) in 1 M KCl buffer. Electrode impedances typically ranged from 200 to 300 MΩ. The recording micropipettes were sometimes beveled slightly (with no reduction in electrode resistance) to facilitate penetration of the inner limiting membrane.

In both *in vitro* preparations, retinal cell bodies were vitally stained by adding a few drops of the fluorescent dye acridine orange (~1 mM solution) to the superfusate as it entered the chamber. The electrode tip and the retina were viewed together under epifluorescence illumination at high resolution with a Zeiss 40× water-immersion objective lens. The fluorescing compound in the micropipette and the acridine fluorescence of neuronal cell bodies were observed with the same filter combination (excitation filter, 410–490 nm; barrier filter, 515 nm). Cell penetration was confirmed by iontophoresis of Lucifer Yellow or Pyranine into the cell. If the cell penetration and recording was successful, Neurobiotin was iontophoretically passed into the cell with positive current (0.1–0.3 nA; ~15 min).

Light stimulation and data acquisition

The amacrine cell light response was recorded using a light emitting diode (LED) based stimulator (Dacey & Lee, 1994; Dacey et al., 1996). This stimulator is similar in design to that used previously in psychophysical studies (Swanson et al., 1987) and in extracellular recordings of ganglion cells from the intact eye of the macaque monkey (e.g. Lee et al., 1990). Light sources were red, green, and blue LEDs (dominant wavelengths, 638, 554 and 445 nm, respectively) mounted on a small optical bench held above the microscope such that the light path was projected through the camera port as a spot on the retinal surface. Size of the stimulus field was varied by use of a diaphragm and by changing the microscope objective. With the 40× water-immersion objective the maximum spot size was 250 μm in diameter. A 4× objective was also used to create a larger field up to 2.5 mm in diameter.

A gamma spectroradiometer was used to measure the light output of the diodes in the plane of the retina. The LEDs were set equal in luminance using psychophysical methods (Dacey & Lee, 1994), and this measure was comparable to equal luminance calculated from the radiometric data. Illuminance at the retinal surface was ~1000 $\mu W/cm^2$ for the combined output of the red and green LEDs and was estimated to correspond to ~1000 photopic trolands. A linear relationship between input voltage and light

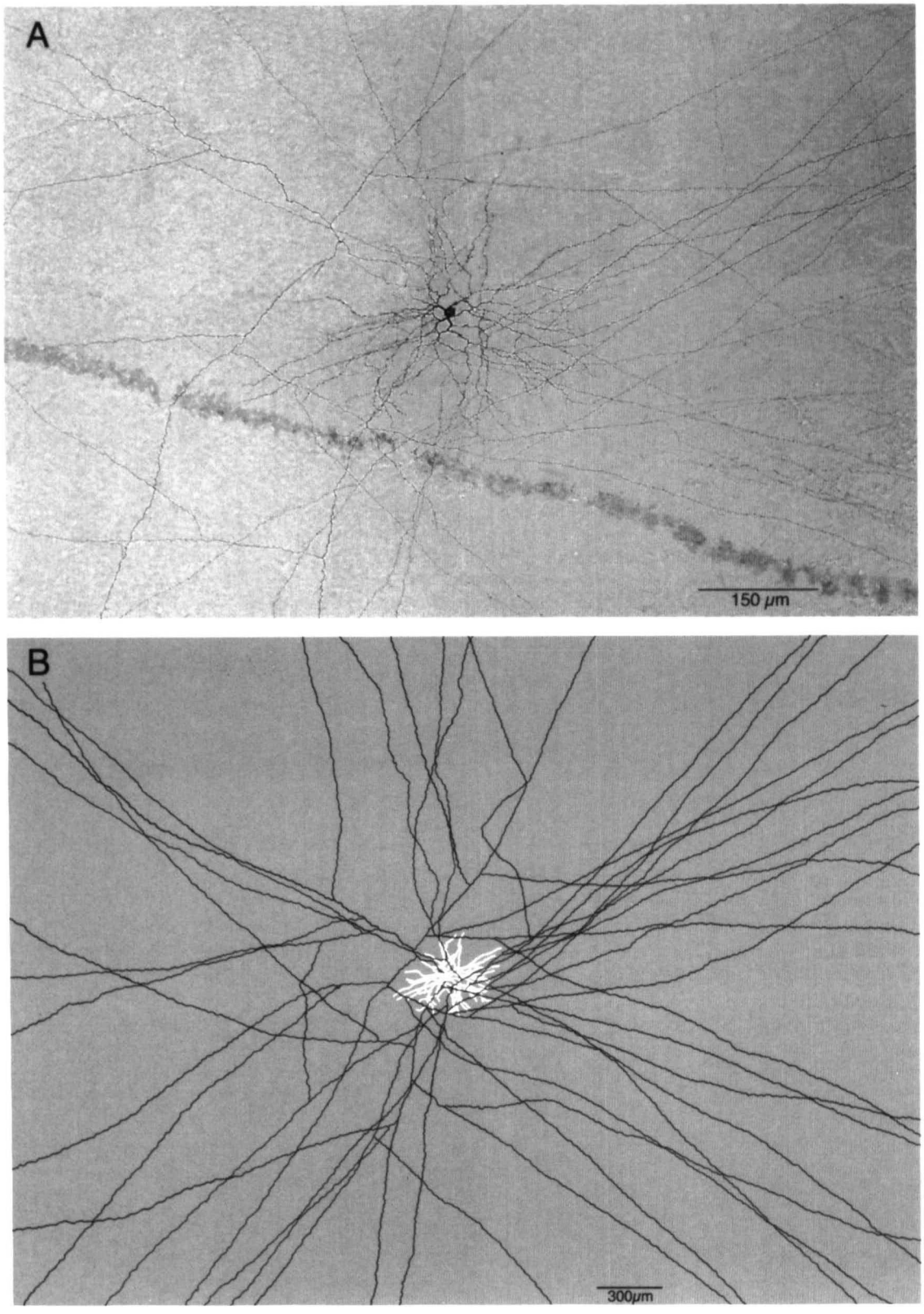

Fig. 1. Morphology of the A1 amacrine cell in macaque retina. (A) Photomicrograph of an A1 cell intracellularly injected with HRP; wholemount preparation with the plane of focus in the inner plexiform layer. The dendritic tree is spiny and highly branched and forms a field ~400 μm in diameter around the cell body. Two axon-like processes arise from proximal dendrites and give rise to a second, more sparsely branching arbor that extends beyond the dendritic field; only the proximal portion of the axon-like arbor is shown in this field. (B) Camera-lucida tracing of the cell shown in (A) at lower magnification. Here a greater extent of the axon-like arbor is illustrated. The dendritic tree is shown in white and the axon-like component is shown in black. The stained axon-like field is ~4.5 mm in diameter.

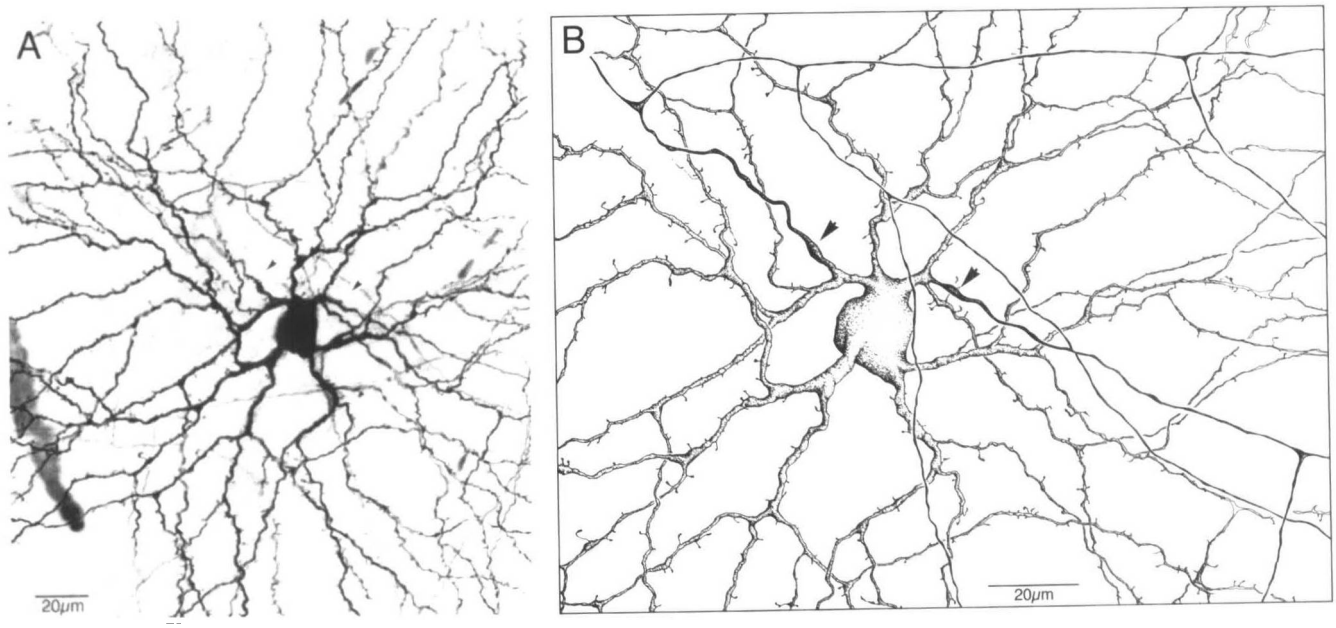

Fig. 2. Comparison of the dendritic and axon-like morphology of the A1 cell. (A) This photomicrograph illustrates the morphology of the proximal dendrites; they are spiny and show a radiate branching pattern. Two axon-like processes originate from proximal dendrites (arrows); note the hillock-like thickening and rapid taper of these processes. (B) A camera-lucida tracing of the same region at higher magnification illustrates the difference in morphology and branching pattern between the dendrites and axon-like processes. The spiny dendrites are lightly stippled and the axon-like processes are filled. Note that the axon-like processes are thin and spine free and may branch at obtuse angles.

output was achieved by frequency modulation of constant amplitude 250-μs pulses. For the present experiments the LED output was modulated in time as square waves; the relative amplitude and phase each of the diodes could be independently controlled to create various luminance modulated stimuli (diodes in phase) or equiluminant chromatic stimuli (diodes run in counterphase). In previous studies, we have used counterphase stimulus waveforms to analyze the chromatic properties and cone photoreceptor inputs to horizontal cells and ganglion cells in the macaque retina *in vitro* (Dacey & Lee, 1994; Dacey et al., 1996). In the present results, we focus on the response of the A1 amacrine cell type to a luminance modulated stimulus.

Receptive-field mapping

Two methods were used to map the spatial extent of the A1 amacrine cell receptive field. The first method provided a one dimensional profile (see Fig. 8); we used a long, narrow-slit aperture placed in the LED light path that produced a stimulus 50 μm in width and 2 mm in length on the surface of the retina. The slit image could be positioned relative to the recorded cell with a manual micropositioner. To map the receptive field, luminance modulation (red and green diodes modulated in phase at 2.44 Hz) was passed through the slit and tested at 80-μm intervals across the receptive field. At each location the stimulus was modulated for ~6 s and the intracellular response was averaged over 2 cycles of the stimulus. A map of responsivity was constructed from the peak values of the average slow potential for ON and OFF excitatory responses. A second map of responsivity was constructed from the average spike frequency (spikes/s) for a 50-ms window beginning with the first spike for both ON and OFF responses.

In the second method, we used a small luminance modulated spot, 150 μm in diameter, to generate a two-dimensional plot of the receptive field (see Fig. 9). The spot was placed at different locations in the cell's receptive field using a motorized *X–Y* positioner under either manual (joystick) or computer control. The joystick was first used to center the spot at the position that appeared to give the largest response; this was taken as the center or zero position. Under computer control, the spot was then moved at 115-μm intervals in a 9 × 9 square matrix of locations around the zero point; the spot thus mapped a square area 920 μm on a side. A response was measured at each of the 81 spot locations. The data were subsequently plotted both as single tracks across the receptive field and as an interpolated surface plot using commercially available software (Spyglass, Transform, Spyglass, Inc., Champaign, IL). Using both the slit and the spot techniques, the diameter of the receptive field was taken to be the diameter of a Gaussian fit to the data, with the diameter defined as width of the curve at the point where responsivity has declined by a factor of e (2.7-fold). In the case of the two-dimensional plot, a Gaussian was fit to the data points that passed through the most responsive part of the field.

Morphological analysis

At the end of an experiment, each retina was fixed for 2 h in phosphate-buffered (0.1 M; pH 7.4) 4% paraformaldehyde and 1% glutaraldehyde (in the case of HRP injections) or buffered 4% paraformaldehyde only (in the case of Neurobiotin injections). An HRP reaction product was displayed in the retinal wholemount using diaminobenzidine (DAB) as the chromagen (Dacey, 1989, 1990*a*). For the Neurobiotin-injected cells, the Vector ABC method (Vector Labs., Burlingame, CA, Elite kit) was used to bind HRP to the Neurobiotin. Retinas were placed in 0.5% tritonX-100 (in 0.1 M phosphate buffer) at room temperature for 3 h, and then incubated in buffer containing the Vector avidin-biotin-HRP complex (~50 μl of kit solution A, ~50 μl of kit solution B in 2.5 ml

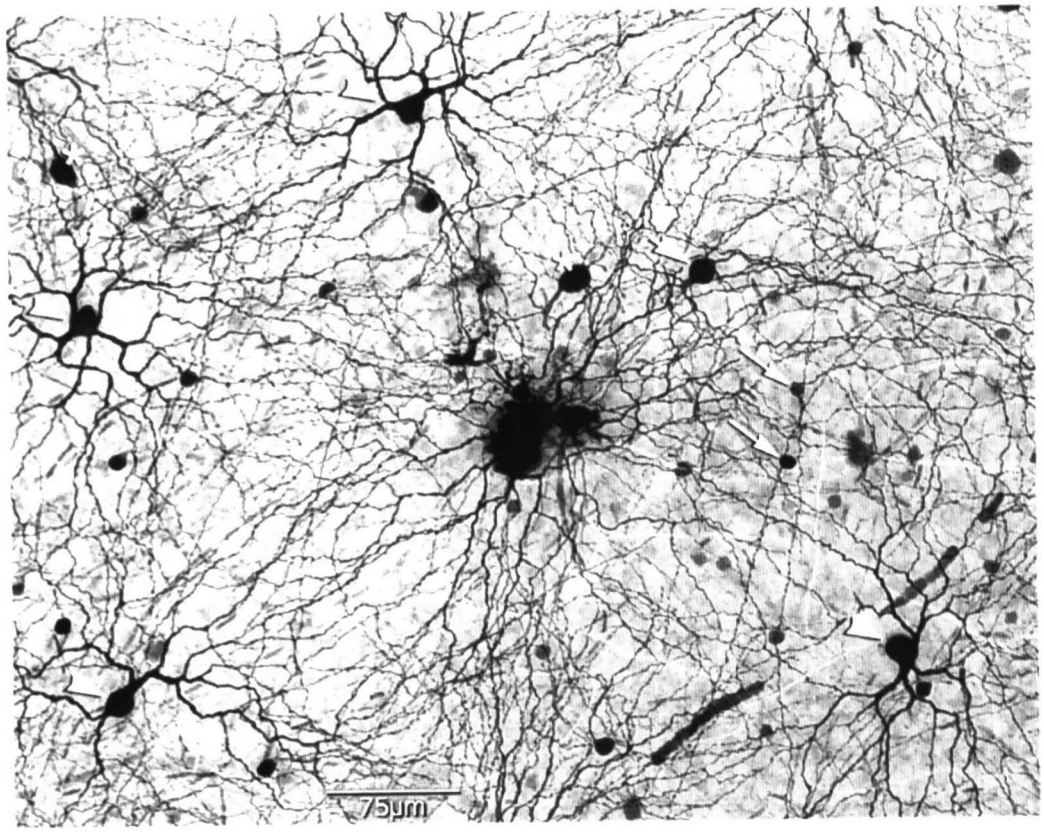

Fig. 3. Pattern of tracer coupling after intracellular injection of Neurobiotin into the A1 amacrine. Injected cell is at center. Tracer coupling was observed in neighboring A1 cells (arrowheads). Heterotypic coupling was also observed in a group of amacrine cells with small cell bodies and sparsely branching dendrites (long arrows), a second group with larger cell bodies (short arrow) and more highly branched dendrites, and a population of ganglion cells with small cell bodies (asterisks) and sparsely branching fields. The ganglion cells were identified by the presence of a single axon arising from the soma and entering the optic fiber layer; they appeared morphologically uniform and regularly arranged indicating that only a single ganglion cell type is tracer coupled to the A1 cell.

of 0.1 M phosphate buffer) for 3 h. The tissue was then rinsed in buffer for 1 h and standard HRP histochemistry was performed using DAB as the substrate for the HRP reaction. In some cases, the reaction product was intensified by incubating the tissue in a dilute solution of Nitro Blue Tetrozolium and exposing it to a strong light source according to the method described by Vaney (1992). Retinas were mounted on microscope slides in a water-based solution of glycerin and polyvinyl alcohol (Heimer & Taylor, 1974) to prevent tissue shrinkage.

Two approaches were used to accurately identify the morphology of a given intracellularly recorded cell. First, as noted above, the impaled cells were labelled with pyranine by iontophoretic injection during recording; notes and simple drawings were made at this time to characterize the cell's dendritic morphology. Second, the locations of the recorded cells, the optic disc, and the fovea were noted in the coordinate system of the microscope stage, and were used after HRP histochemistry to locate the recorded cell.

Somal areas were measured using a computer graphics tablet and expressed as the diameter of a circle with the equivalent area. To calculate dendritic field area a convex polygon was traced around the dendritic-field perimeter. Dendritic-field diameter was expressed as the diameter of a circle with an equivalent area.

The depth of stratification in the inner plexiform layer was compared for A1 cells with cell bodies located in the inner nuclear layer (n = 4), inner plexiform layer (n = 3), and ganglion cell layer (n = 3). Depth measurements were read from the microscope focus knob (calibrated to 1-μm intervals) for the innermost and outermost dendrites, and the inner nuclear layer and ganglion cell layer borders. The dendritic measurements were then converted to percentage depth within the inner plexiform layer.

Morphological and physiological data base

The anatomical data presented in this study are derived from intracellular staining of 256 A1 amacrine cells; the small data base (n = 64) used in Dacey (1989) has been included. Combined anatomical-physiological identification was achieved in a further 77 A1 cells; of these 77 recorded cells complete receptive-field maps were obtained for 13 cells.

Results

Our first goal was to reliably identify A1 amacrine cells *in vitro*, record their light responses, and test the hypothesis that the A1 cell is a spiking amacrine. Our second goal was to measure the A1's receptive-field size and test the hypothesis that the receptive field corresponded in extent to the compact, spiny dendritic tree.

The A1 cell has distinct axon-like and dendritic components

As previously shown, several features of the A1 amacrine cell allow it to be easily targeted for intracellular recording and staining

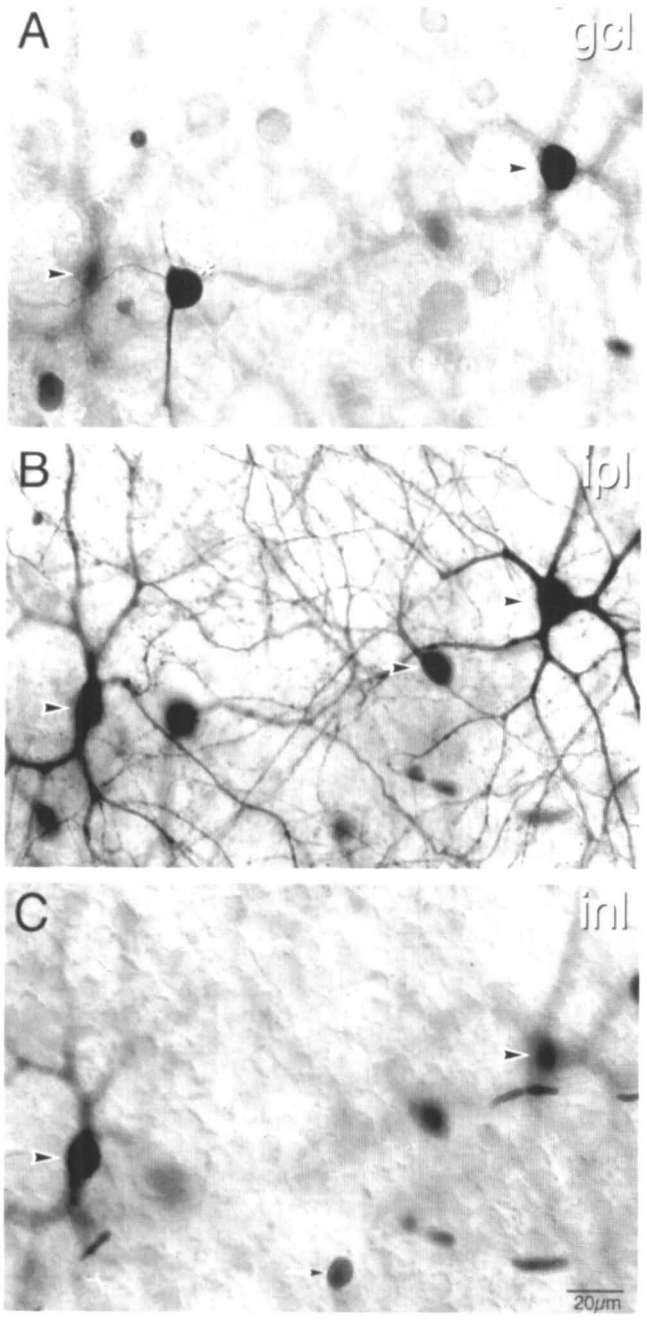

Fig. 4. A1 cells form a single, regularly arranged mosaic but their cell bodies can be located in the inner nuclear layer, inner plexiform layer, or ganglion cell layer. Two neighboring A1 cells labelled by Neurobiotin tracer coupling are shown at different depths of focus in panels A, B, and C (arrowheads). (A) Plane of focus in the ganglion cell layer (gcl); A1 cell on the right is located in gcl. Tracer-coupled ganglion cell is indicated by the asterisk. (B) Plane of focus in the inner plexiform layer (ipl); dendritic plexus is in focus; tracer-coupled amacrine with medium-sized soma is indicated by the short arrow. (C) Plane of focus shifted to the inner nuclear layer (inl) A1 cell body on the left is located in the inl; long arrow indicated tracer-coupled amacrine with small cell body.

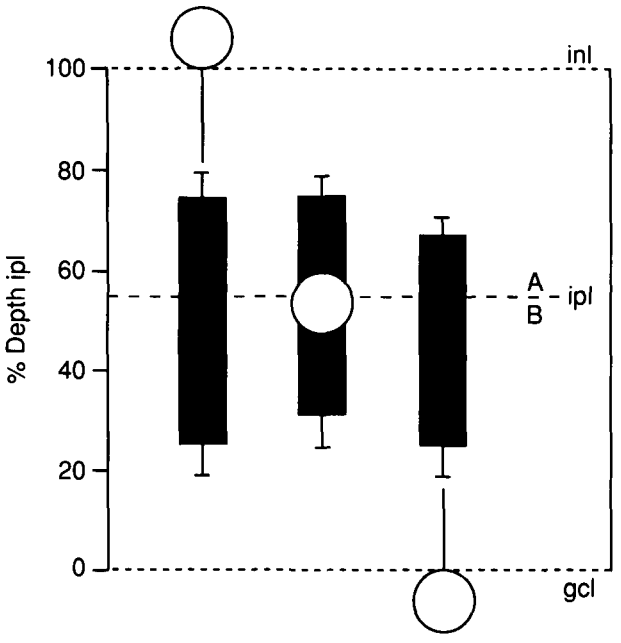

Fig. 5. Depth of stratification of the A1 cell plexus. Processes were broadly stratified in the middle third of the inner plexiform layer. Somata located in the inner plexiform layer (ipl), inner nuclear layer (inl), or ganglion cell layer (gcl) contributed to a single plexus. The shaded areas indicate the location of the outermost and innermost dendrites (n = 3 cells in each position) as a percentage of the depth of the ipl; one standard deviation is indicated by the short lines extending from the shaded bars. Location of the cell body for each cell group is indicated by the circle associated with each shaded bar.

in the *in vitro* retina (Dacey, 1989). When the retina is stained with acridine orange the cell body of the A1 cells can frequently be observed in the middle of the inner plexiform layer. In addition, with some practice it is also possible to recognize A1 cell bodies in the inner nuclear layer; they have larger cell bodies than most other amacrine cells (~15–20 μm diameter) and a more conspicuous nucleus than the surrounding cell bodies. The characteristic stout and spiny dendrites and the slender axon-like processes that arise from them can be easily recognized when these cells are filled with dye and observed microscopically *in vitro*.

When an A1 cell is intracellularly filled with HRP, the dual axon-like and dendritic morphologies are fully revealed and can be best illustrated at low magnification (Figs. 1A and 1B). The compact branching of the dendritic tree and the more sparse branching of the axon-like tree that arises from and surrounds the dendritic tree is shown in Fig. 1A. The stained portion of the axon-like tree of the same cell is more fully shown at much lower magnification in a camera-lucida tracing (Fig. 1B). The axon-like component (shown in black) has a diameter of ~4.5 mm; by contrast the dendritic tree (shown in white) has a diameter of ~420 μm. No terminations for the axon-like processes could be observed; the HRP reaction product was traced distally until it gradually faded, indicating that these processes form a field that must be even larger than shown here.

The contrast between the morphology of the axon-like processes and the dendritic tree is seen clearly at higher magnification (Figs. 2A and 2B). In this HRP-filled cell, two axon-like processes originate from thick primary dendrites close to the soma (arrows, Figs. 2A and 2B). The dendrites are tortuous and spiny, and branch at acute angles to form an overall radiate pattern. Each axon-like process typically shows a hillock-like thickening at its origin and then tapers to a thin and smooth process; branching is sparse and often at right or obtuse angles. As the axon-like processes extend beyond the dendritic tree, they become studded with small boutons.

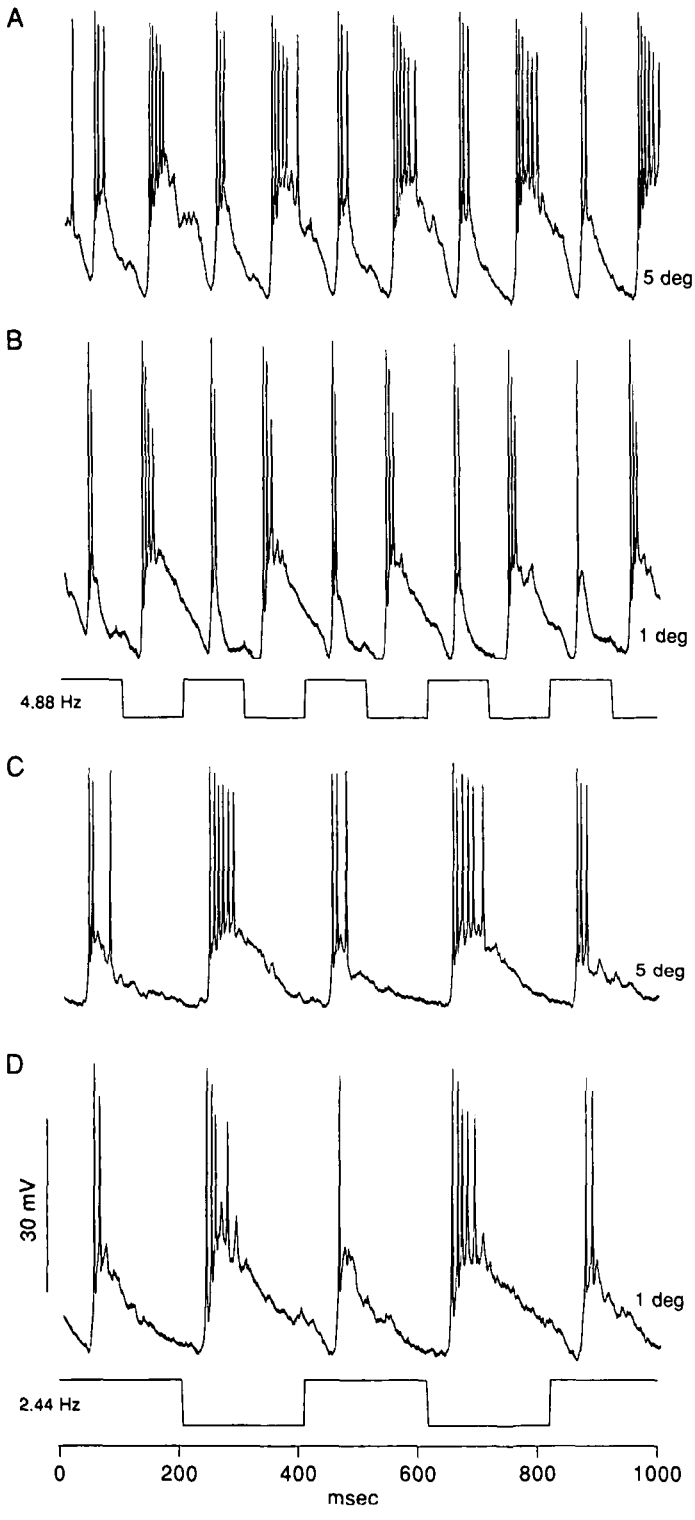

Fig. 6. Intracellularly recorded light response of the A1 amacrine cell. The A1 gives a transient ON–OFF response characterized by a phasic burst of fast large-amplitude spikes at both light onset and offset. (A) Synaptic potential modulation and associated spike discharge in response to a 5-deg field flickered at 4.88 Hz, light stimulus = log −2.0. (B) Response to a 1-deg field; light stimulus = log 0.0; stimulus waveform (in phase modulation of red and green LEDs) is shown directly beneath synaptic potential. (C) Response to a 5-deg field modulated at 2.44 Hz; stimulus intensity = log −1.0. (D) Response to a 1-deg field; stimulus intensity = log 0.0; stimulus waveform is shown directly beneath synaptic potential.

Mosaic of A1 cells: Homotypic tracer coupling

We reexamined the morphology of the A1 cell using intracellular injections of the tracer Neurobiotin. Because of its small size, Neurobiotin can be used in high-resistance micropipettes and thus is compatible with intracellular recording from small retinal neurons. In addition, the use of Neurobiotin as an intracellular tracer has revealed an unexpectedly high degree of tracer coupling among diverse amacrine cell types (Vaney, 1992, 1994), so it was likely that intracellular injection of Neurobiotin would provide new information about mosaic organization of A1 cells and their links to other retinal neurons. Not surprisingly, when A1 cells were injected with Neurobiotin a striking and extensive pattern of tracer coupling was revealed (Fig. 3). Neighboring A1 amacrine cells (homotypic coupling) were darkly stained (arrowheads, Fig. 3), with typically 2–3 tiers of A1 cells stained; homotypic staining gradually faded with distance from the injected cell and the size of a typical patch of tracer coupled A1 dendritic trees was about 2 mm in diameter. The homotypic coupling also showed clearly that the A1 soma could be located in either the ganglion cell layer,

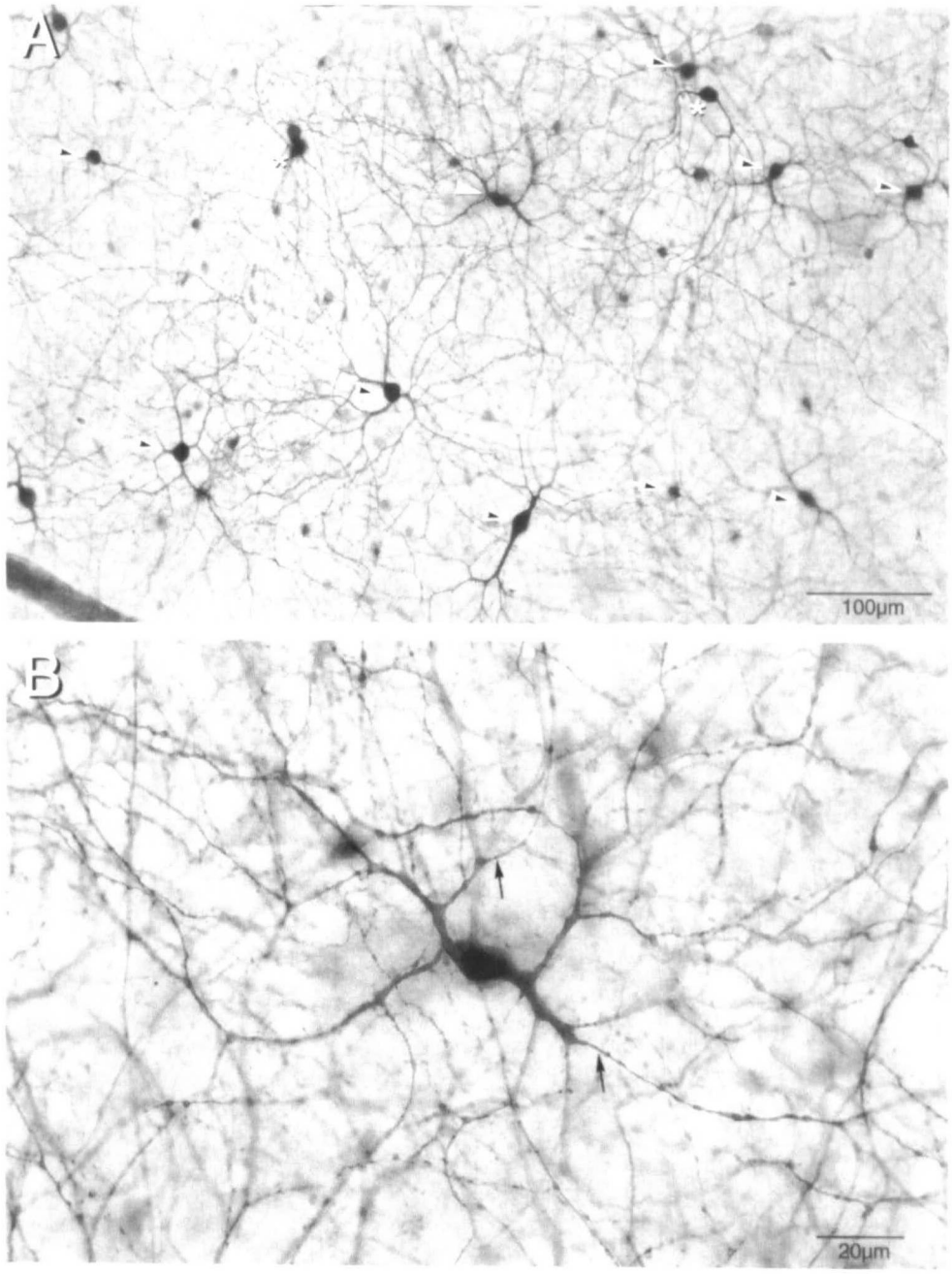

Fig. 7. Intracellular Neurobiotin injection of A1 cell whose light response and receptive-field map is illustrated in Fig. 8. (A) Tracer coupling pattern is typical for A1 cells; compare with Fig. 3. Recorded cell is indicated by the white arrowhead. (B) Higher magnification of the cell that was recorded from; origins of axon-like processes are indicated by the arrows. A simple tracing of the dendritic tree of this cell is shown in Fig. 8A.

the inner plexiform layer or the inner nuclear layer (Figs. 4A–4C). However, the regularity of the spacing between neighboring cells suggested an orderly mosaic of a single cell type. The mean ± S.D. nearest-neighbor distance for 76 cells taken from five A1 patches was 157 ± 31.4 μm. If an index of regularity is taken as the ratio of the mean neighbor distances to the standard deviation (Wässle & Riemann, 1978), the A1 cells have a regularity of 5.1, a degree of regularity comparable to that of the highly regular H1 horizontal cells of the primate (Wässle et al., 1989).

If the A1 cell bodies in the inner nuclear, inner plexiform, and ganglion cell layers are all part of a single functional array, then their processes should all costratify in the inner plexiform layer. To determine if this was the case, the stratification depth of the dendritic processes was determined for the A1 cell bodies in each of the three layers (n per group = 3). There was some variability in the depths of the innermost and outermost dendrites; however, the A1 cells in the ganglion cell layer, inner plexiform layer, and inner nuclear layer all costratified in the central third of the inner plexiform layer (Fig. 5). Thus, regardless of soma position, we conclude that the A1 cells comprise a single cell type and a single, regularly arranged mosaic.

A1 cell density was calculated from seven patches of labeled cells. There was a mean of 21 cells per square millimeter (range = 30–13 cells/mm^2) in the retinal periphery (covering a retinal ec-

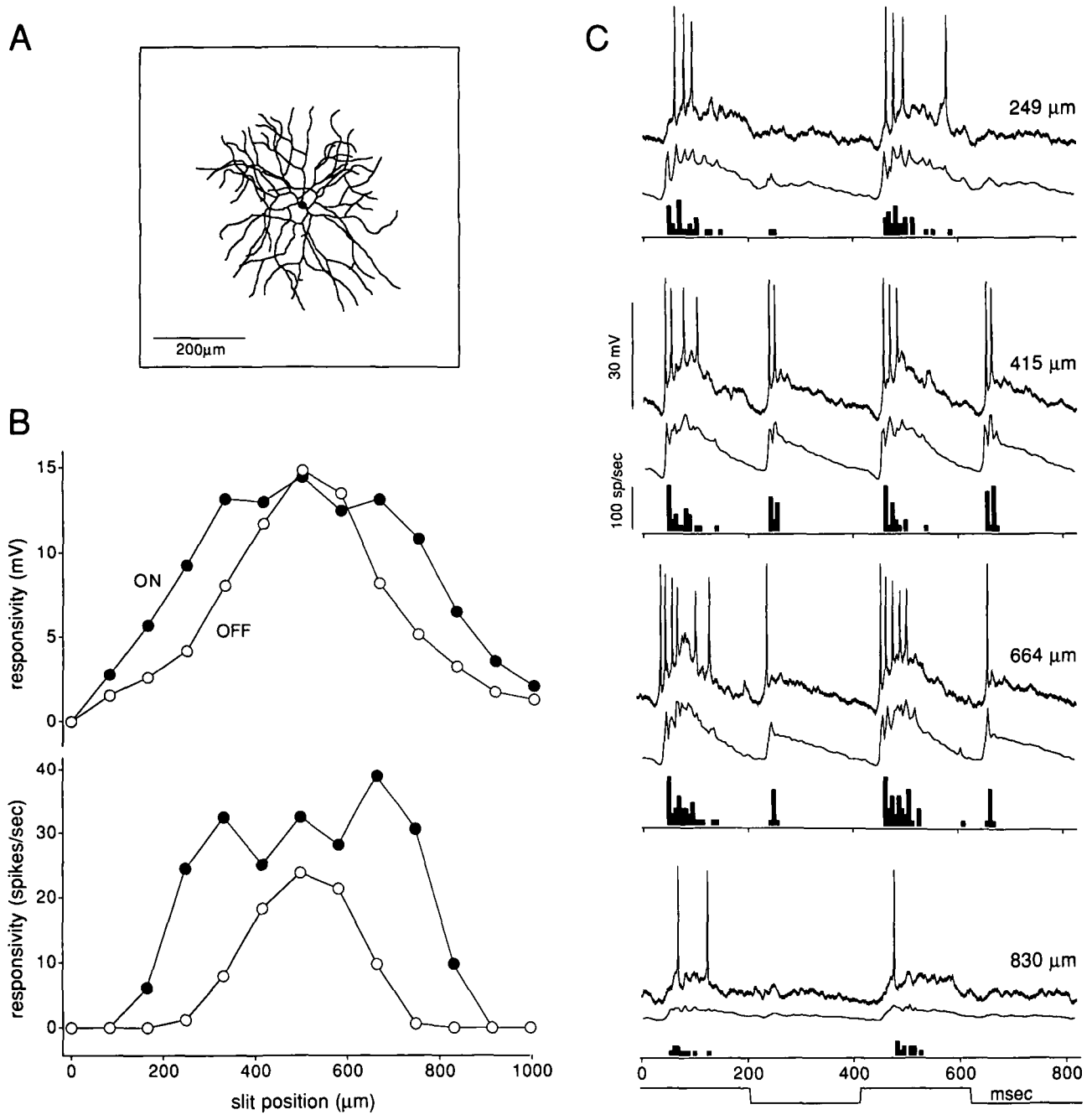

Fig. 8. A1 amacrine cell receptive-field map. (A) Dendritic tree outline of recorded A1 cell; photomicrograph shown in Fig. 7. (B) Receptive-field maps were made by moving a 50-μm-wide bar of light through the receptive field at 83-μm intervals; at each bar location the stimulus was square wave modulated at 2.44 Hz. Upper plot, cell responsivity based on the peak amplitude of the slow depolarizing potential averaged over 6.4 s stimulus modulation at each bar location; ON response, solid symbols; OFF response, open symbols. Lower plot, second map of same receptive field based on spike discharge (spike frequency was determined for a 50-ms window after initial spike). (C) Examples of cell responses at four locations in the receptive field. At each position a single record is shown of the slow potential and associated spike discharge for two cycles of the stimulus (top trace). The lower trace shows an average of the response over entire duration of stimulus, and below this is a poststimulus time histogram of spike discharge. Slit postion is given to the right of each record.

centricity range of 6.5–14.9 mm from the fovea). Average coverage (coverage = density in cells/mm^2 × dendritic-field area in mm^2) of 2.8 was provided by the spiny dendritic trees and contrasted with a minimal coverage of 720 for the widespreading axon-like arbors.

Heterotypic tracer coupling

In addition to the homotypic coupling, Neurobiotin injection into A1 cells revealed tracer coupling to at least two other amacrine cell types and a single ganglion cell type (Fig. 3). The two amacrine

Table 1. *Comparison of dendritic-field diameter (μm) to the ON and OFF components of the receptive field mapped with either narrow slits or small spots*

Dendritic field	Receptive field: Spike discharge ON	Spike discharge OFF	Synaptic potential ON	Synaptic potential OFF	Mapping method
300	462	307	561	442	slit
375			408	424	slit
			714	416	slit
350	200	216	425	451	slit
508			644	409	slit
412	660	319	737	466	slit
			1000	593	slit
			707	551	slit
420	303	303	271	423	spot-grid
550	511	533	804	886	spot-grid
360	392	576	598	830	spot-grid
430	294	206	587	505	spot-grid
400	251	293	405	402	spot-grid
Mean 412	385	344	604	522	
±S.D. 78	153	136	196	159	
rf: *df*[a]	1.1	1.0	1.6	1.4	

[a]Mean field diameter (μm) + 1 S.D.

cell types could be distinguished from each other by a large difference in soma diameter; the more frequently seen type had a small soma (mean ± S.D. = 9.5 ± 1.0; n = 37; Fig. 3; long arrows), the other had a larger soma (mean ± S.D. = 12.4 ± 1.1; n = 15; Fig. 3, short arrows). Both of these amacrines had soma diameters that did not overlap with the much larger bodied A1 cells (mean ± S.D. = 16.3 ± 2.3; n = 35). Both amacrine types appeared to have large, moderately branching dendritic trees though no attempt was made to study the fine details of their morphology. The ganglion cell type was clearly distinguished by the presence of a single axon that emerged from the cell body and projected away from the patch in the optic fiber layer (asterisks, Fig. 3). The ganglion cell bodies were somewhat smaller than the A1 cells (mean ± S.D. = 14.8 ± 1.5; n = 15). All of the ganglion cells were similar in morphology, with large, sparsely branching dendritic trees and a regular distribution within the Neurobiotin-labelled patch, suggesting that the A1 cells are coupled to a single morphologically distinct ganglion cell type.

Light response of the A1 cell

The intracellularly recorded light response of the A1 cell to a luminance-modulated stimulus is illustrated for four different cells in Figs. 6A–6D. A graded slow potential and an associated spike discharge are elicited at both onset and offset of the stimulus. This ON–OFF response was characteristic of all the A1 cells recorded and morphologically identified (n = 77). The ON–OFF nature of the response was independent of light level over 3 log units in the high photopic range. The spectral sensitivity and temporal-frequency response of the cell suggested that most, if not all, of the response was cone mediated at the light levels used. The light response was also unaffected by stimulus size ranging from ~150 μm to 2 mm in diameter. The overall temporal-frequency response of the ON and OFF components was somewhat different, an issue to be considered elsewhere; over the low-to-middle frequencies reported here (0.5–10 Hz) both phases of the response behaved similarly. The ON–OFF nature of the cone response is consistent with the broad stratification of the A1 cell dendritic tree across the border between the ON and OFF subdivisions of the inner plexiform layer (Fig. 5).

The details of both the spike potentials and graded response components were also consistent from cell to cell: upon cell penetration the physiological signature of the A1 light response was as readily recognized as its distinctive morphology. The slow potential had a fast rise time at both stimulus onset and offset; the synaptic potential was typically more sustained (with a slow decay to resting) during the OFF phase than during the ON phase of the response. The action potentials were fast and large in amplitude ranging from 30 to 60 mV. Variation in spike height appeared to be related to the quality of the penetration and the intracellular recording rather than to any real differences across the sampled cells. Cells that showed no injury discharge, stable resting membrane potentials (~−60 mV in the dark) and were recorded for long periods (1–7 h) all had large-amplitude spikes that overshot 0 mV. Small-amplitude "dendritic" spikes as observed in other amacrine cell types in nonmammalian retina (Miller & Dacheux, 1976) and more recently in amacrine cells of the rabbit retina (Bloomfield, 1992) were never observed in the A1 response. The spike discharge was typically initiated on the fast, rising phase of the slow potential response; a burst of spikes was observed at both ON and OFF with the ON discharge being somewhat more phasic than the OFF discharge. From 3–10 spikes were observed in a burst with an instantaneous frequency of up to ~150 spikes/s. In several stable penetrations the A1 cells also showed a sluggish maintained spike discharge of ~3–5 spikes/s.

Receptive-field size and structure

The A1 cell showed a phasic ON–OFF light response to both large- and small-field stimuli. Because the A1 cell's dendrites extend across the ON–OFF subdivision of the inner plexiform layer, it is likely that these cells receive excitatory input from both the ON and OFF cone bipolar pathways. As would be predicted from such a circuitry, the A1 receptive field is characterized by coextensive ON and OFF excitatory response regions. In ten A1 cells, it was possible to map completely both the ON and OFF receptive fields and also to recover the complete dendritic morphology of the recorded cell (in a few other cases tracer coupling was so extensive that it was impossible to clearly sort out the dendritic processes of the recorded cell). One example of a cell whose receptive field was mapped is illustrated in Figs. 7 and 8. The filled cell showed the characteristic A1 tracer coupling pattern when injected with Neurobiotin (Fig. 7A). The spiny dendritic tree could be distinguished from the axonal processes and the dendritic processes of neighboring cells (Fig. 7B); the dendritic tree was 410 μm in diameter (Fig. 8A). Receptive-field diameters were determined independently for both the spiking response and the amplitude of the slow potential (Figs. 8B and 8C). The two measures gave about the same overall receptive-field size, though some modulation of the membrane potential below spike threshold was present. For the cell shown in Fig. 8, the receptive-field diameter was 660 μm for the ON response and 320 μm for the OFF response; in most cases, however, the ON and OFF response fields were more similar in size (Table 1; e.g. Fig. 10).

To gain a more complete picture of the A1 receptive field and its relation to the dendritic field, we also obtained two-dimensional

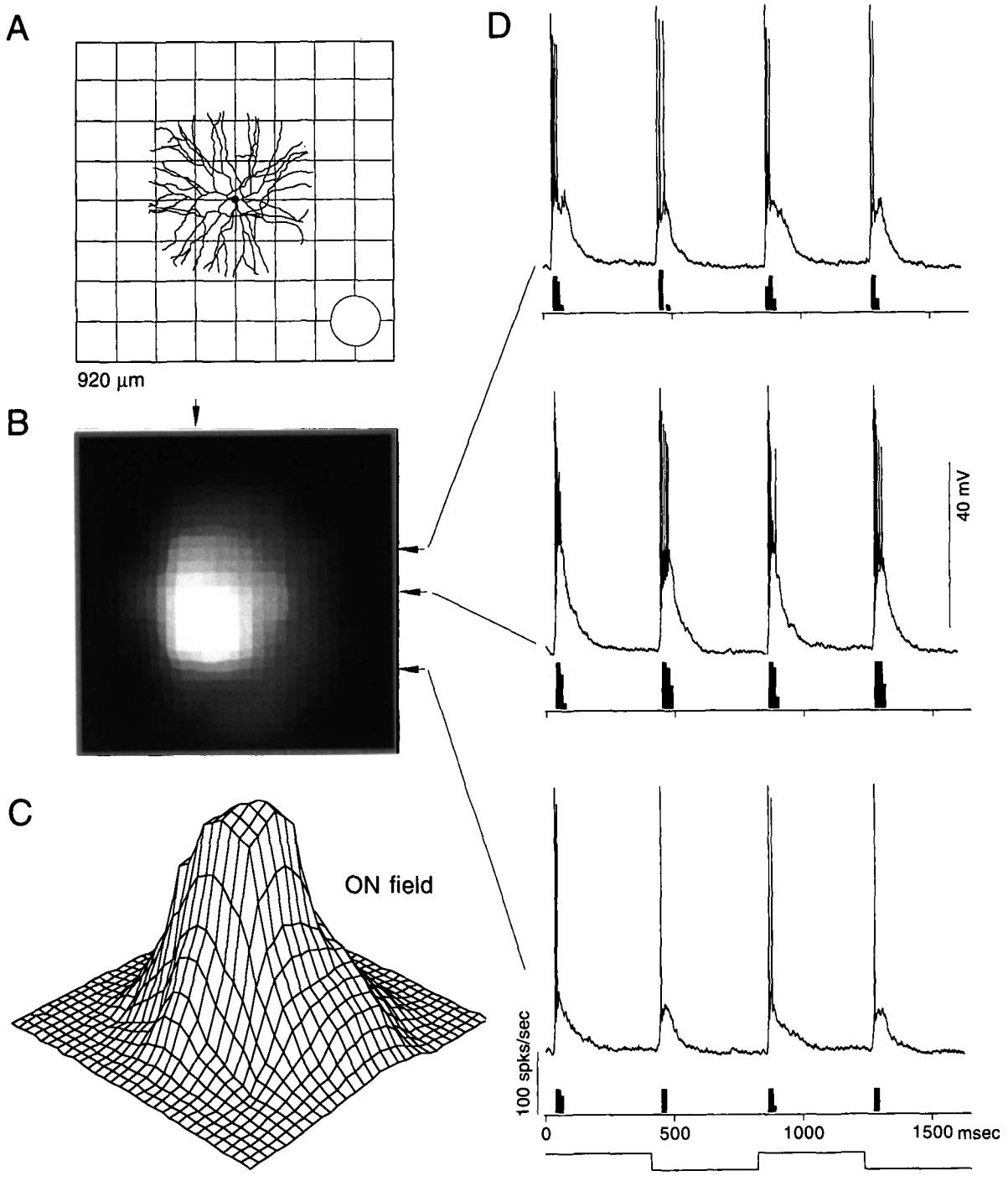

Fig. 9. Two-dimensional receptive-field map of an A1 amacrine cell. (A) Tracing of dendritic tree outline is shown in relation to square grid of points used to map receptive field. Light responses were recorded at 81 locations in a 920-μm square field; stimulus spot (inset at lower right of grid) was 150 μm in diameter and was moved along the grid in 115 μm intervals. (B) Interpolated image of responsivity across the mapped square for the ON spiking response component only; responsive region is circular and concentrated over the dendritic tree. (C) Surface plot of image shown in (B); the ON spiking receptive-field diamter for this cell was 294 μm. (D) Examples of intracellular records taken at three different locations in the receptive-field map. Stimulus locations are indicated by the arrowed points in (B): the intersections of a vertical line dropped from the top arrow with horizontal lines extended from the three side arrows give the three locations. Slow potential and associated spike discharge for two stimulus cycles are shown, together with a poststimulus time histogram of spike discharge.

receptive-field maps from five morphologically characterized A1 cells (Table 1) using the spot mapping method outlined in Fig. 9. Maps were again made for the ON and OFF components of both the slow potential and the spike discharge. A comparison of those maps for one cell having a dendritic-field diameter of 400 μm is illustrated in Fig. 10. The receptive fields were circular and symmetrical; the fields defined by the synaptic potential were ~1.5 times the diameter of the fields defined by the

spike discharge. All the fields are reasonably well fit by a Gaussian function. The size of the fields defined by the synaptic potentials approximated the dendritic-field size; the spiking fields were somewhat smaller.

Neither the bar nor the two-dimensional spot mapping methods revealed evidence of an inhibitory surround in the receptive field. We have used the same procedures to map the receptive fields of macaque ganglion cells in which a clear surround response can be

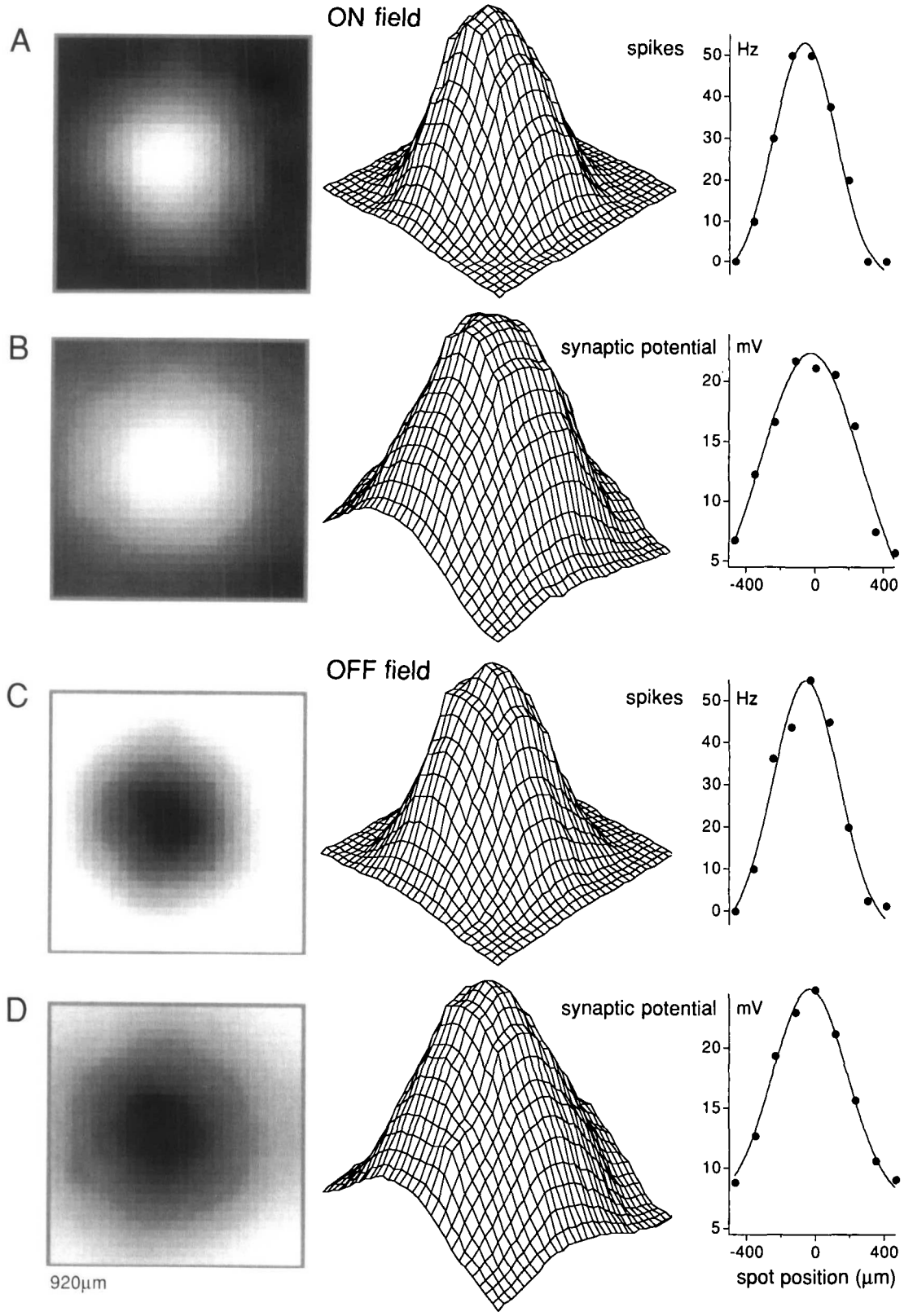

FIGURE 10.

elicited when a bar or spot is moved outside of the receptive-field center (unpublished observations). Similarly, annuli were ineffective in revealing any clear surround response in A1 cells but very effectively reveal surrounds in other primate amacrine and bipolar cells (unpublished observations).

The overall relationship between receptive-field, dendritic-field, and axonal-field diameter is summarized in Table 1 and Figs. 11 and 12. The A1 dendritic-field sizes of the physiologically mapped cells fell within the cluster of measured dendritic fields for the total anatomical data base of 256 cells. On average the spiking fields were ~10% larger than the dendritic trees, and the fields defined by the synaptic potentials were ~50% larger. There is variation in the data set, with some spiking fields being larger and others being smaller than the dendritic field. However, even the largest receptive fields were an order of magnitude smaller than the diameter of the axon-like arbors.

Discussion

Topography and morphology of the A1 amacrine cell network

Intracellular injection of Neurobiotin revealed several new features about the A1 amacrine cells not appreciated in the previous anatomical study (Dacey, 1989). First, the location of A1 cell bodies is variable: A1 cell bodies are found in the amacrine cell layer, the inner plexiform layer, or the ganglion cell layer. Regardless of soma depth, the spatial array of neighboring cells is regular and the dendritic processes all stratify at the same depth in the inner plexiform layer suggesting strongly that the A1 cells correspond to a single morphological type with a characteristic mosaic distribution across the retina. Second, the spatial density of the A1 cells is revealed by tracer coupling after intracellular injection of Neurobiotin. In the retinal periphery there are ~20 A1 cells/mm^2; this is a much lower density than the AII, rod amacrine cells (~800 cells/mm^2; Wässle, et al., 1995) or the cholinergic, starburst amacrine cells (~350 cells/mm^2; Rodieck & Marshak, 1992) but about twice the density of the dopaminergic amacrine cell (~10 cells/mm^2; Dacey, 1990*a*). If the relative proportions of the different amacrine types are roughly similar across mammalian species, as seems likely (review: Vaney, 1990), then the A1 amacrine cells would make up less than 0.5% of all amacrine cells in macaque retina. Third, the dendritic and axon-like processes of the A1 cells appear to cover the retina independently of one another, reinforcing the idea that these processes are functionally distinct. The spiny dendritic trees of the A1 cell economically tile the retina with a low mean coverage like that commonly observed in many ganglion cell types (Wässle & Boycott, 1991). By contrast, the axon-like processes do not appear to neatly tile the retina but extend freely for long distances across the fields of many neighboring cells. Whether the axon-like processes interact to form a second, larger scale organization is not clear. Finally, the A1 cells are tracer coupled to at least two other amacrine cell types and a single ganglion cell type. Unfortunately, these coupled cells do not provide any clues to the functional role of the A1 cell. The coupled amacrines, like the A1 cell, were also relatively low in density and were not recognized morphologically as any previously described amacrine types. Similarly, the coupled ganglion cell type does not appear to be a previously characterized type in primate retina (Rodieck, 1988; Dacey, 1996). Thus, the A1 cell may be an intriguing component in one of the many ganglion cell microcircuits in the primate that remains to be characterized.

Spiking physiology of the A1 cell

How does the light-evoked response of the A1 cell fit with current understanding of spiking amacrine cell physiology? An early classification scheme for amacrine cell spikes in nonmammalian retina, based on the assumption that amacrine cells are axonless, divided spikes into small-amplitude (5–10 mV) "dendritic" spikes, and single, large-amplitude "somatic" spikes (Miller & Dacheux, 1976). Both types of transient depolarizations were shown to be mediated by sodium currents as they were abolished by the sodium channel blocker tetrodoxin. The small-amplitude transients were assumed to originate in the dendrites and propagate toward the soma, some electrotonic decay perhaps accounting for their small and variable size. Single somatic spikes were suggested to be triggered by the dendritic spikes, and their larger amplitude was thought to reflect proximity to the recording electrode. More recently somatic and dendritic amacrine spikes were observed in rabbit retina; some rabbit amacrine cells were also shown to have repetitive spike discharge (Bloomfield, 1991, 1992, 1996). How these different sorts of spiking behaviors map onto the approximately 40 morphologically distinct amacrine cell subpopulations is unclear.

The A1 amacrine cell also has large-amplitude, repetitive spike discharge, apparently corresponding to the "somatic" spikes, and lacks the "dendritic" spikes of the above scheme. From our results and those of other recent studies, we speculate that the different classes of spiking behavior occur in different amacrine cell types: with the repetitive, larger amplitude "somatic" spikes in axon-bearing amacrines and the smaller "dendritic" spikes in axonless amacrines. Smaller amplitude presumed "dendritic" spikes have been observed in at least two amacrine cell types that lack a distinct axon-like component: the serotonin-accumulating S1 cell and the cholinergic starburst amacrine (Bloomfield, 1992). The morphology of other rabbit amacrines with large-amplitude spikes has not been studied in detail so the question of whether they show axonal components comparable to the A1 cell remains open. In one recent study, recordings were made from a small number of ON–OFF amacrine cells in cat retina, one of which showed axon-like processes (Freed et al., 1996); these cells did *not* show large-amplitude spikes; however, the maximum amplitude of the light-evoked slow potential was extremely small (~1–3 mV) suggesting that these cells may have been damaged by the electrode penetra-

Fig. 10. Comparison of two-dimensional receptive-field maps based on synaptic potential and spike discharge. (A) Interpolated image and surface plot for ON spiking field (plot made as illustrated in Fig. 9); plot to the right shows the responsivity in spikes/s along a line through the most responsive part of the receptive field. The data points are fit with a Gaussian curve; receptive-field diameter, taken as the diameter of the Gaussian, is 511 μm. (B) Image and surface plots as in (A) for the averaged ON synaptic potential. Receptive-field diameter diameter for ON synaptic potential determined as for (A) is 804 μm. (C) Image and surface plots for the OFF spiking component of the receptive field; it is coextensive in size and location and similar in responsivity to the ON component; receptive-field diameter, 533 μm. (D) Image and surface plots for the OFF synaptic potential; receptive-field diamter 886 μm. For both the ON and OFF fields, the receptive field defined by the synaptic potential was ~1.6 times the diameter of the field derived from the spike discharge. Dendritic-field diameter for this cell was 550 μm.

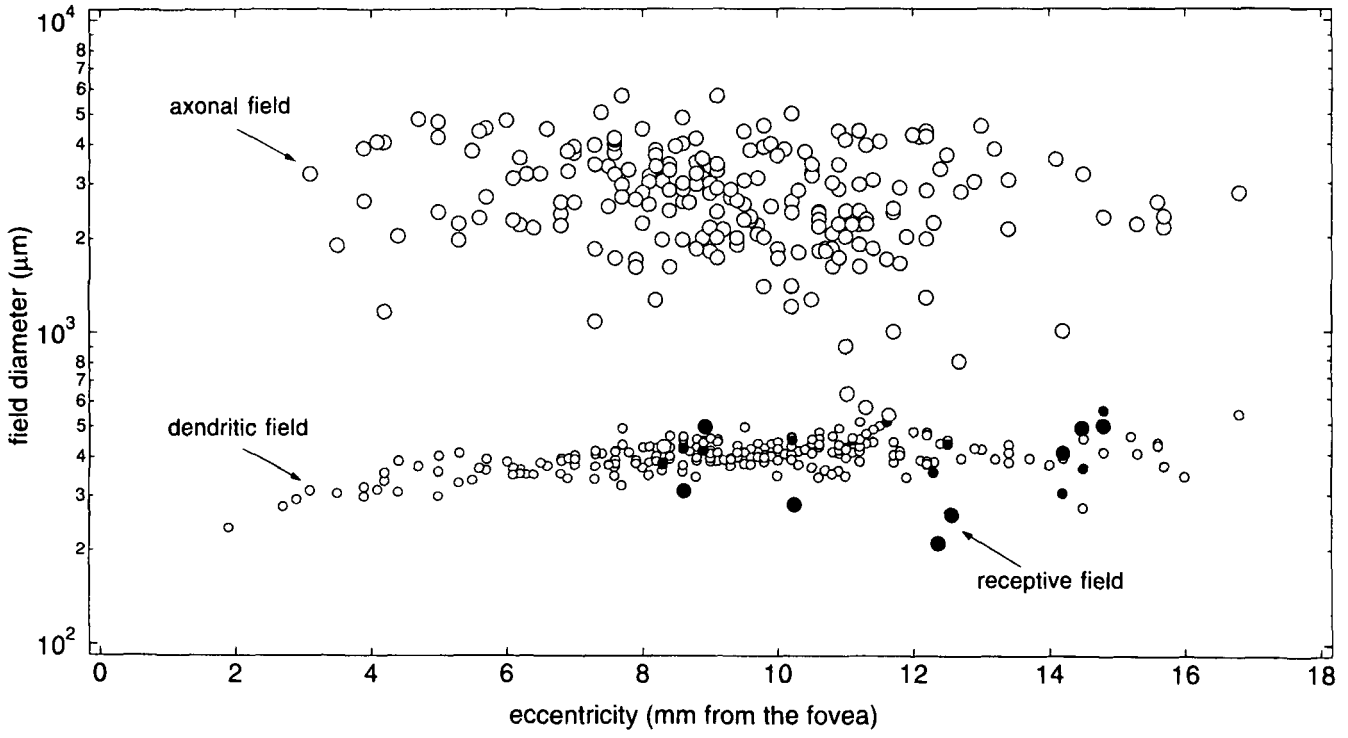

Fig. 11. Scatterplot of dendritic-field, axonal-field, and receptive-field sizes of A1 amacrine cells. Dendritic fields of the A1 cells that were recorded physiologically (small black circles) fell within the cluster of dendritic-field diameters derived from other A1 cells that were characterized only anatomically (small open circles). Receptive-field sizes (mean of ON and OFF components) derived from the synaptic potential and spike discharge are indicated by the light gray circles and dark gray circles, respectively. Axonal-field diameter (large open circles) for the A1 cells was about a factor of 10 greater than receptive-field diameter. The general relationship between dendritic field, axonal field, and receptive field is illustrated pictorially in Fig. 12.

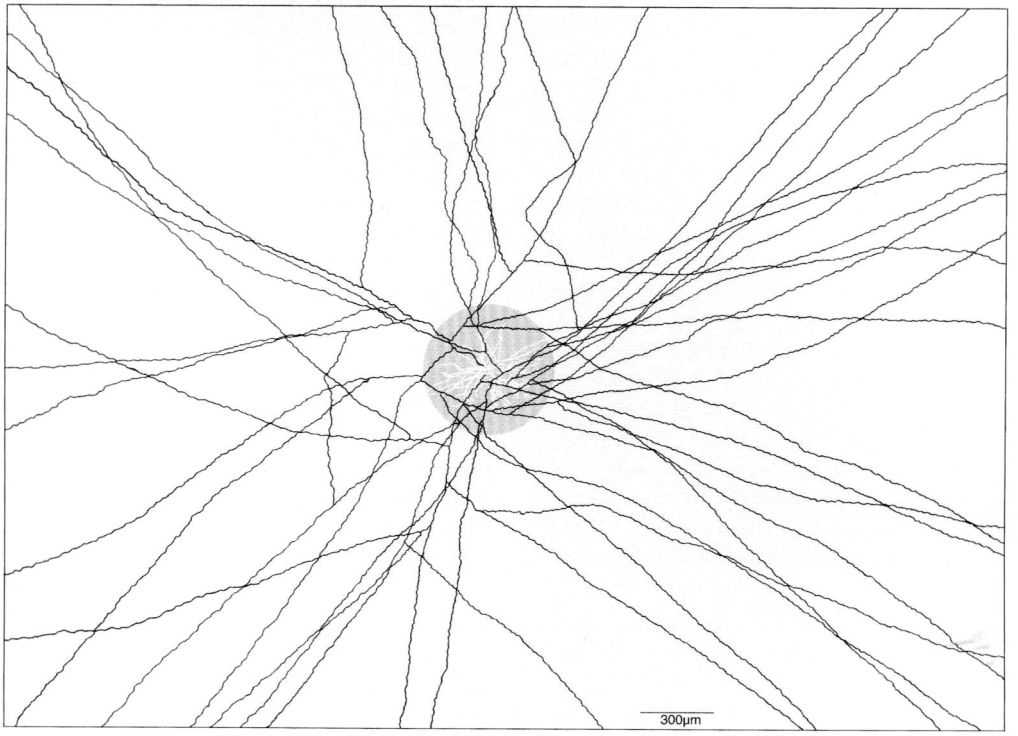

Fig. 12. The receptive-field diameter of the A1 cell is comparable in extent to the diameter of the spiny dendritic tree (compare with Fig. 1B). The mean receptive-field size of the A1 cells mapped in this study (gray circle) has been superimposed on a camera-lucida tracing of the dendritic (in white) and axon-like fields (in black) of the A1 cell. The receptive-field diameter determined by spike discharge is on average about 10% larger than the highly branched and spiny dendritic tree see Table 1). The sparsely branching, axon-like arbor, by contrast, gives rise to a field that is at minimum, 4–5 mm in diamter.

tion. In our experience, when an A1 cell (or a ganglion cell) is damaged by a poor electrode penetration (which we can directly confirm by visual inspection of dye filling during the recording) the membrane potential is depolarized, spikes are absent or greatly reduced, and the amplitude of the light-evoked slow potential is greatly reduced.

The present results provide no direct evidence as to the precise location of spike initiation in the A1 cells but the presence of large-amplitude, repetitive spike discharge, recorded from the soma very near the origin of distinctive axon hillock-like structures, suggests that rather than being "somatic" spikes, these spikes could be generated by the axonal component of the cell and propagate distally throughout the widespreading axon-like arbor. The receptive-field maps of the A1 cell are consistent with this view: receptive-field size approximates dendritic-field size but is an order of magnitude smaller than the massive, widespreading axonal arbor (Figs. 11 and 12). Since the axon-like processes do not appear to provide a pathway for excitatory input to the cell body or proximal dendrites, we speculate that they are presynaptic, output structures as their light-microscopic morphology intimates. It is also equally possible that the axon-like processes are made up of local input–output compartments in electrical isolation from the recording electrode, in analogy with the axon terminal system of the mammalian axon-bearing horizontal cells. A difficulty with this alternative speculation is that the striking repetitive spike discharge recorded at the soma remains enigmatic. By contrast, the axonal spiking hypothesis is a simple interpretation of both the physiology and anatomy and makes an equally simple and testable anatomical prediction: synaptic inputs to the A1 cell should be confined to the spiny dendritic tree, and synaptic outputs to the axon-like arbor.

Acknowledgments

Supported by NIH Grants EY06678 (D.M.D), EY06471 (D.K.S.), EY01730 (Vision Research Core), and RR00166 to the Regional Primate Center at the University of Washington. We thank Keith Boro and Pat Dacey for technical assistance. We are especially grateful to Joel Pokorny and Vivianne Smith for help in setting up the LED stimulus, to Barry B. Lee for designing data acquisition and analysis software, to Steve Buck for help with photometry, and to Kate Mulligan and Helen Sherk for their continued contributions and support.

References

AMMERMÜLLER, J. & WEILER, R. (1989). Correlation between electrophysiological responses and morphological classes of turtle retinal amacrine cells. In *Neurobiology of the Inner Retina—NATO ASI Series, Vol. H31*, ed. WEILER, R. & OSBORNE, N.N., pp. 117–132. Berlin-Heidelberg: Springer-Verlag.

BLOOMFIELD, S.A. (1991). Two types of orientation-sensitive responses of amacrine cells in the mammalian retina. *Nature* **350**, 347–350.

BLOOMFIELD, S.A. (1992). Relationship between receptive and dendritic field size of amacrine cells in the rabbit retina. *Journal of Neurophysiology* **68**, 711–725.

BLOOMFIELD, S.A. (1996). Effect of spike blockade on the receptive-field size of amacrine and ganglion cells in the rabbit retina. *Journal of Neurophysiology* **75**, 1878–1893.

CATSICAS, S., CATSICAS, M. & CLARKE, P.G.H. (1987). Long-distance intraretinal connections in birds. *Nature* **326**, 186–187.

COOK, P.B. & WERBLIN, F.S. (1994). Spike initiation and propagation in wide field transient amacrine cells of the salamander retina. *Journal of Neuroscience* **14**, 3852–3861.

DACEY, D.M. (1988). Dopamine-accumulating retinal neurons revealed by *in vitro* fluorescence display a unique morphology. *Science* **240**, 1196–1198.

DACEY, D.M. (1989). Axon-bearing amacrine cells of the macaque monkey retina. *Journal of Comparative Neurology* **284**, 275–293.

DACEY, D.M. (1990*a*). The dopaminergic amacrine cell. *Journal of Comparative Neurology* **31**, 461–489.

DACEY, D.M. (1990*b*). Distinct cell types in living macaque retina display an unexpected granular fluorescence. *Society for Neuroscience Abstracts* **16**, 466.

DACEY, D.M. (1990*c*). The dopaminergic amacrine cells of the cat retina. *Investigative Ophthalmology and Visual Science* (Suppl.) **31**, 535.

DACEY, D.M. (1996). Circuitry for color coding in the primate retina. *Proceedings of the National Academy of Sciences of the U.S.A.* **93**, 582–588.

DACEY, D.M. & BRACE, S. (1992). A coupled network for parasol but not midget ganglion cells in the primate retina. *Visual Neuroscience* **9**, 279–290.

DACEY, D.M. (1993). The mosaic of midget ganglion cells in the human retina. *Journal of Neuroscience* **13**, 5334–5355.

DACEY, D.M. & LEE, B.B. (1994). The "blue-on" opponent pathway in primate retina originates from a distinct bistratified ganglion cell type. *Nature* **367**, 731–735.

DACEY, D.M., LEE, B.B., STAFFORD, D.K., POKORNY, J. & SMITH, V.C. (1996). Horizontal cells of the primate retina: Cone specificity without spectral opponency. *Science* **271**, 656–659

DJAMGOZ, M.B.A., DOWNING, J.E.G., KIRSCH, M., PRINCE, D.J. & WAGNER, H.-J. (1988). Plasticity of cone horizontal cell functioning in cyprinid fish retina: Effects of background illumination of moderate intensity. *Journal of Neurocytology* **17**, 701–710.

DJAMGOZ, M.B.A., DOWNING, J.E.G. & WAGNER, H.-J. (1989). Amacrine cells in the retina of a cyprinid fish: Functional characterization and intracellular labelling with horseradish peroxidase. *Cell and Tissue Research* **256**, 607–622.

DJAMGOZ, M.B.A. & VALLERGA, S. (1989). Structure-function correlation: Amacrine cells of fish and amphibian retinae. In *Neurobiology of the Inner Retina—NATO ASI Series, Vol. H31*, ed. WEILER, R. & OSBORNE, N.N., pp. 195–208. Berlin Heidelberg: Springer-Verlag.

FAMIGLIETTI, E.V. (1990). A new type of wide-field horizontal cell, presumably linked to blue cones, in rabbit retina. *Brain Research* **535**, 174–179.

FAMIGLIETTI, E.V. (1992*a*). Polyaxonal amacrine cells of rabbit retina: PA2, PA3, and PA4 cells. Light and electron microscopic studies with a functional interpretation. *Journal of Comparative Neurology* **316**, 422–446.

FAMIGLIETTI, E.V. (1992*b*). Polyaxonal amacrine cells of rabbit retina: Morphology and stratification of PA1 cells. *Journal of Comparative Neurology* **316**, 391–405.

FAMIGLIETTI, E.V., JR. (1983). 'Starburst' amacrine cells and cholinergic neurons: Mirror-symmetric on and off amacrine cells of rabbit retina. *Brain Research* **261**, 138–144.

FREED, M.A., PFLUG, R., KOLB, H., NELSON, R. (1996). ON–OFF amacrine cells in cat retina. *Journal of Comparative Neurology* **364**, 556–566.

HEIMER, C.V. & TAYLOR, C.E.D. (1974). Improved mountant for immunofluorescent preparations. *Journal of Clinical Pathology* **27**, 254–256.

JENSEN, R.J. (1995). Receptive-field properties of displaced starburst amacrine cells change following axotomy-induced degeneration of ganglion cells. *Visual Neuroscience* **12**, 177–184.

KANEKO, A. (1970). Physiological and morphological identification of horizontal bipolar and amacrine cells in goldfish retina. *Journal of Physiology* **207**, 623–633.

LEE, B.B., POKORNY, J., SMITH, V.C., MARTIN, P.R. & VALBERG, A. (1990). Luminance and chromatic modulation sensitivity of macaque ganglion cells and human observers. *Journal of Optical Society of America A* **7**, 2223–2236.

MAGUIRE, G., LUKASIEWICZ, P. & WERBLIN, F. (1989). Amacrine cell interactions underlying the response to change in the tiger salamander retina. *Journal of Neuroscience* **9**, 726–735.

MATSUMOTO, N. & NAKA, K.I. (1972). Identification of intracellular responses in the frog retina. *Brain Research* **42**, 59–71.

MILLER, R.F. & DACHEUX, R. (1976). Dendritic and somatic spikes in mudpuppy amacrine cells: Identification and TTX sensitivity. *Brain Research* **104**, 157–162.

MILLER, R.F. & BLOOMFIELD, S.A. (1983). Electroanatomy of a unique amacrine cell in the rabbit retina. *Proceedings of the National Academy of Sciences of the U.S.A.* **80**, 3069–3073.

PETERS, B.N. & MASLAND, R.H. (1996). Responses to light of starburst amacrine cells. *Journal of Neurophysiology* **75**, 469–480.

RODIECK, R.W. (1988). The primate retina. In *Comparative Primate Biology, Vol. 4: Neurosciences*, ed. STEKLIS, H.D., pp. 203–278. New York: Alan R. Liss, Inc.

RODIECK, R.W. & MARSHAK, D.W. (1992). Spatial density and distribution

of choline acetyltransferase immunoreactive cells in human, macaque, and baboon retinas. *Journal of Comparative Neurology* **321**, 46–64.

SAGAR, S.M. (1987). Somatostatin-like immunoreactive material in the rabbit retina: Immunohistochemical staining using monoclonal antibodies. *Journal of Comparative Neurology* **266**, 291–299.

SWANSON, W.H., UENO, T., SMITH, V.C. & POKORNY, J. (1987). Temporal modulation sensitivity and pulse-detection thresholds for chromatic and luminance perturbations. *Journal of the Optical Society of America* **4**, 1992–2005.

TAUCHI, M. & MASLAND, R.H. (1984). The shape and arrangement of the cholinergic neurons in the rabbit retina. *Proceedings of the Royal Society B* (London) **223**, 101–119.

TAYLOR, W.R. (1996). Response properties of long-range axon-bearing amacrine cells in the dark-adapted rabbit retina. *Visual Neuroscience* **13**, 599–604.

TAYLOR, W.R. & WÄSSLE, H. (1995). Receptive field properties of starburst cholinergic amacrine cells in the rabbit retina. *European Journal of Neuroscience* **7**, 2308–2321.

TERANISHI, T., NEGISHI, K. & KATO, S. (1987). Functional and morphological correlates of amacrine cells in carp retina. *Neuroscience* **20**, 935–950

VANEY, D.I., PEICHL, L. & BOYCOTT, B.B. (1988). Neurofibrillar long-range amacrine cells in the mammalian retinae. *Proceedings of the Royal Society B* (London) **235**, 203–219.

VANEY, D.I. (1990). The mosaic of amacrine cells in the mammalian retina. *Progress in Retinal Research* **9**, 49–100.

VANEY, D.I. (1992). Photochromic intensification of diaminobenzidine reaction product in the presence of tetrazolium salts: applications for intracellular labelling and immunohistochemistry. *Journal of Neuroscience Methods* **44**, 217–223.

VANEY, D.I. (1994). Patterns of neuronal coupling in the retina. In *Progress in Retinal and Eye Research*, ed. OSBORNE, N.N. & CHADER, G.J., pp. 301–355. Great Britain: Pergamon Press Ltd.

WÄSSLE, H. & BOYCOTT, B.B. (1991). Functional architecture of the mammalian retina. *Physiological Reviews* **71**, 447–480.

WÄSSLE, H., BOYCOTT, B.B. & RÖHRENBECK, J. (1989). Horizontal cells in the monkey retina: Cone connections and dendritic network. *European Journal of Neuroscience* **1**, 421–435.

WÄSSLE, H., GRÜNERT, U., CHUN, M.H. & BOYCOTT, B.B. (1995). The rod pathway of the macaque monkey retina: Identification of AII-amacrine cells with antibodies against calretinin. *Journal of Comparative Neurology* **361**, 537–551.

WÄSSLE, H. & RIEMANN, H.J. (1978). The mosaic of nerve cells in the mammalian retina. *Proceedings of the Royal Society B* (London) **200**, 441–461.

WERBLIN, F. & DOWLING, J.E. (1969). Organization of the retina of the mudpuppy, *Necturus maculosus* II Intracellular recording. *Journal of Neurophysiology* **32**, 339–355.

WERBLIN, F.S. (1972). Lateral interactions at inner plexiform layer of vertebrate retina: Antagonistic response to change. *Science* **175**, 1008–1010.

WERBLIN, F.S. & COPENHAGEN, D.R. (1974). Control of retinal sensitivity III. Lateral interactions at the inner plexiform layer. *Journal of General Physiology* **63**, 88–110.

WHITE, C.A., CHALUPA, L.M., JOHNSON, D. & BRECHA, N.C. (1990). Somatostatin-immunoreactive cells in the adult cat retina. *Journal of Comparative Neurology* **293**, 134–150.